Journal of The Electrochemical Society, **160** (2) A344-A350 (2013)
0013-4651/2013/160(2)/A344/7/$28.00 © The Electrochemical Society

Oxygen Reduction Reaction Using MnO_2 Nanotubes/Nitrogen-Doped Exfoliated Graphene Hybrid Catalyst for Li-O_2 Battery Applications

Hey Woong Park,[a] Dong Un Lee,[a] Linda F. Nazar,[b] and Zhongwei Chen[a,z]

[a]*Department of Chemical Engineering, Waterloo Institute for Nanotechnology Waterloo Institute for Sustainable Energy, University of Waterloo, Waterloo, Ontario N2L 3G1, Canada*
[b]*Department of Chemistry, Waterloo Institute for Nanotechnology, University of Waterloo, Waterloo, Ontario N2L 3G1, Canada*

Nitrogen-doped thermally exfoliated graphene (NExG) synthesized by a simple one-step method combined with α-MnO_2 nanotubes (NT) is employed as air cathode materials for lithium oxygen (Li-O_2) battery applications. α-MnO_2 NT/NExG composite is shown to demonstrate excellent oxygen reduction reaction (ORR) activity in an aprotic non-aqueous electrolyte Li-O_2 cell resulting in 2.92 V at the current density of 100 mA g^{-1}, discharge current density of 7.2 A g^{-1} at 2.2 V, and the maximum power density of 15.8 W g^{-1} based on carbon mass. This excellent performance of the composite suggests that not only α-MnO_2 NT exhibits a remarkable catalytic activity for ORR, but also NExG with a large surface area and high electrical conductivity is capable of catalyzing ORR, demonstrating an outstanding hybrid effect in an aprotic non-aqueous electrolyte Li-O_2 cell.
 [DOI: 10.1149/2.086302jes]

Manuscript submitted October 23, 2012; revised manuscript received November 28, 2012. Published December 14, 2012.

The use of highly marked price and limited reservoir of fossil fuel, which causes environmental issues such as global warming, is directing the scientific community to continually explore alternative energy conversion and storage systems. Since vehicular applications are the primary consumer of the oil reservoir, it is imperative that a highly efficient alternative energy source is developed for the transportation systems. Recently, lithium–ion (Li-ion) battery, as the most advanced energy storage device amongst the commercialized energy sources, have been the major alternative energy source of electric vehicles (EVs) and hybrid electric vehicles (HEVs). However, current Li-ion battery technology with the energy density of only 160 Wh kg^{-1} is inadequate for the ultimate long-term needs of the EVs. Along with the development of Li ion batteries with higher voltage cathode materials, and novel anode materials such as Si and Sn, lithium-oxygen (Li-O_2) batteries have drawn much attention from the scientific community, which have led Abraham et al. to introduce a practical rechargeable Li-O_2 battery with polymer electrolyte in 1996.[1] Later in 2006, Bruce et al. proposed a viable Li-O_2 battery using an organic electrolyte for Li ion battery prompted research effort in Li-O_2 batteries as a major stream.[2] Interestingly, both the theoretical and practical energy densities of a Li-O_2 battery (11680 Wh kg^{-1} and 1700 Wh kg^{-1}, respectively) are comparable to those of a combustion engine.[3] For this reason, the Li-O_2 batteries are regarded as one of the most promising candidates for the future energy source in EVs, offering the potential for researchers in this field to be innovative.[4–6] However, a few hurdles of Li-O_2 battery such as insufficient cycle stability, low energy efficiency, and poor discharge rate capability remain to be addressed before commercialization of the batteries. These challenges of Li-O_2 batteries are directly related to oxygen reduction reaction (ORR) due to its slow reaction rate, which has a significant impact on the desired power and energy density of Li-O_2 batteries. Therefore, the development of a highly efficient ORR catalyst in an aprotic non-aqueous medium is a research area of much interest in order to improve the discharge performance, enhance the rate capability, and lower the overpotentials.[7,8]

Graphene-based materials have received continued attention for applications in energy conversion and storage systems due to the unique properties such as large surface area (> 2600 m^2 g^{-1}), outstanding electrical conductivity (as high as 2200 S m^{-1}), and unique 2-D planar morphology.[9–11] The extraordinary characteristics of graphene has not only been promoting fundamental research, but also have provided opportunity in improving the performance of the Li-O_2 batteries. For example, a distinct 2-D nanostructure of graphene have shown a remarkable catalytic activity for ORR in both aqueous and aprotic electrolytes,[12,13] especially when graphene is doped with heterogeneous nitrogen atoms because of the increased catalytic active sites from the defects and functional groups.[14–17] According to a literature, nitrogen-doped graphene demonstrated 40% higher specific capacity than that of the pristine graphene in the Li-O_2 battery.[14] Moreover, it has been extensively investigated in combination with various metal oxides to create graphene/metal oxide composite materials with enhanced electrochemical activities for Li-O_2 batteries.[18,19]

In this report, for the first time, nitrogen-doped exfoliated graphene (NExG) and alpha (α) phase MnO_2 nanotube (NT) composite is introduced as an ORR active air cathode material for non-aqueous Li-O_2 battery applications. The graphene sheets in NExG with a high electrical conductivity facilitate charge transfer by providing electron pathways for the air cathode. Furthermore, unique morphology of the graphene sheets allows increased O_2 diffusion through the sheets for the accumulation of lithium peroxide (Li_2O_2) in the cathode during battery discharge.[13,14] NExG hence plays important roles of being a highly conductive support with the capabilities to act an as electrocatalyst itself. Amongst various metal oxides, α-MnO_2 is a very attractive catalyst material due to its notable benefits such as low cost, environmental benignity, abundance and catalytic activity toward ORR in both aqueous and non-aqueous electrolytes.[20,21] The mechanism of ORR using MnO_2 in an alkaline electrolyte have been previously investigated, however it is still unclear as different valence states of Mn depend on the crystal structure.[22] MnO_2 supported on various carbon matrices have also been studied in a non-aqueous electrolyte Li-O_2 batteries, which showed remarkable activity toward ORR.[21,23] However, to the best of our knowledge, MnO_2 with nanotube morphology has not been evaluated in an aprotic non-aqueous electrolyte Li-O_2 battery. This unique morphology of MnO_2 NT with a higher surface area than that of MnO_2 nanorods with the same diameter can enhance O_2 utilization during ORR. Furthermore, the crystallographic structures of MnO_2 have been shown to have influence on the catalytic activity toward ORR with α-MnO_2 outperforming β- and γ-MnO_2.[24] In the study, therefore, we introduce a novel α-MnO_2 NT/NExG composite as an air cathode material, and demonstrate that it performs excellent catalytic activity toward ORR in terms of both onset potential and discharge current density in a non-aqueous electrolyte Li-O_2 cell through electrochemical rotating disk electrode (RDE) studies.

Experimental

MnO_2 NT were prepared hydrothermally at 140°C for 12 hour using $KMnO_4$ by a method described in detail elsewhere.[20] The sample

[z]E-mail: zhwchen@uwaterloo.ca

was washed with de-ionized water and dried overnight before use. One step exfoliated and nitrogen-doped exfoliated graphene (ExG and NExG, respectively) were synthesized using graphene oxide (GO) prepared by a modified Hummer's method. To prepare ExG, a certain amount of GO is placed in a quartz tube outside of the heating zone of the horizontal tube furnace. Under 100 sccm of Ar gas flow, when the furnace is heated to 1000°C, the quartz tube is moved along the furnace to bring GO to the heating zone in the center of the furnace. This rapid increase in temperature allows the sheets in GO to be exfoliated and become thermally reduced. After 30 seconds, the tube is shifted back to the initial position outside of the heating zone of the furnace. For the synthesis of NExG, similar procedure is carried out but Ar/NH_3 mixed gases flow of 50 sccm is applied at 900°C and GO is left in the heating zone for 1 hour to allow for nitrogen-doping. After 1 hour, the quartz tube is moved back to the initial position and cooled down under 100 sccm of Ar gas flow. When the furnace temperature is lower than 30°C, the sample is obtained from the quartz tube. The MnO_2 NT/ExG and MnO_2 NT/NExG and MnO_2 NT/Vulcan carbon XC-72 (VC) composites were prepared by mixing the MnO_2 NT and the various carbon materials in a 2:3 weight ratio by a vortex mixer for 20 minutes.

To characterize the synthesized materials in this study, X-ray diffraction (XRD) was utilized to investigate the phase of MnO_2 and the change in the d-spacing of the graphene-based materials. Scanning electron microscopy (SEM) (LEO FESEM 1530) and transmission electron microscopy (TEM) (JEOL 2010F) were used to examine the morphology and surface structure of MnO_2 NT and NExG. X-ray photoelectron spectroscopy (XPS) (Thermal Scientific K-Alpha XPS spectrometer) was carried out to detect the atomic composition of elements in the NExG.

To investigate the electrochemical behaviors of the catalysts for Li-O_2 batteries, ORR activities in an aprotic electrolyte were tested using a potentiostat (CH Instrument 760D) and a rotation speed controller (Pine Instrument Co., AFMSRCE) for a rotating disk electrode (RDE) voltammetry measurement. Glassy carbon disk electrodes (5 mm OD) coated with 15 μL of 4 mg mL^{-1} of the three different MnO_2 NT/carbon composites as described above and VC suspension made by mixing with 0.5 wt% lithiated Nafion in ethanol were used as a working electrode and Li metal was used as a counter and reference electrode. The loading on the glassy carbon is around 0.31 mg cm^{-2}. To examine carbon-free MnO_2 electrode, 2 μL with the same concentration of the suspension was coated on the glassy carbon disk electrode. 1 M $LiPF_6$ in tetra (ethylene) glycol dimethyl ether (TEGDME) is used as the organic electrolyte. The Li-O_2 cells were fabricated in Ar-filled glove box (H_2O < 0.5 ppm, O_2 < 0.5 ppm). The CV curves were recorded from 3.1 to 2.0 V at a scan rate of 5 mV s^{-1} with O_2-saturated electrolyte under electrode rotation speed of 900 RPM.

Results and Discussion

After the synthesis of MnO_2 NT and NExG, the phase of MnO_2 and the degree of d-spacing of NExG after reduction of GO are investigated by X-ray diffraction (XRD) patterns as shown in Figure 1. The XRD pattern of MnO_2 (Figure 1a) confirms alpha phase MnO_2 (α-MnO_2), consistent with the previously reported work.[20,25] α-MnO_2 have been reported to show a superior electrocatalytic activity toward ORR due to its favorable atomic structure compared to the birnessite phase.[20] Figure 1b presents typical XRD pattern of NExG with a broad diffraction peak for (002) plane in the range 22 ∼ 27° associated with the average d-spacing of graphene layers,[26–28] and the inset of Figure 1b shows the XRD pattern of GO produced by the modified Hummer's method with a relatively sharp peak at ∼ 11.5°.[26] The increase in the diffraction angle of NExG compared to that of GO is indicative of the enlargement in the d-spacing of GO sheets due to the oxygen groups that are reduced to form graphene sheets by the one-step NExG process.

Figure 2a shows SEM images of NExG with a voile-like morphology of the graphene sheets suggesting that the one-step exfoliation nitrogen doping process was successfully.[29,30] Furthermore, a TEM image of NExG in Figure 2b presents a similar 2-dimensional surface morphology of the graphene sheets observed in the SEM image, reinforcing the evidence of a successful formation of exfoliated and nitrogen-doped graphene sheets.[27,29] The morphology of the synthesized MnO_2 NT is revealed by SEM as shown in Figure 2c, which clearly shows open ended tubes as an evidence that they are hollow with a cross-section distance in the range from 50 to 100 nm.[20] Figure 2d shows a TEM image of MnO_2 NT which reveals 20 ∼ 23 nm of the wall thickness, and total thickness of ∼70 nm. Moreover, the TEM image shows a difference in contrast between the wall and core of MnO_2 NT, which is another indication that they are formed into nanotube structures. To investigate the elemental composition and varify the nitrogen content and configurations of the graphene structures, X-ray photoelectron spectroscopy (XPS) characterization is conducted. The main peak of C 1s at 284.1 eV in the full XPS spectrum (Figure 2e) is an indication of the sp2 configuration suggesting most of carbons are set in the conjugated honeycomb lattice.[15,16,31] Two other peaks at 398.1 and 532.1 eV correspond to N 1s and O 1s, respectively, which confirms that NExG is composed of nitrogen, carbon and oxygen atoms.[15,16] The presence of N 1s peak is a strong evidence that the heterogeneous nitrogen atoms are successfully doped into the graphene sheets. The spectrum reveals the atomic

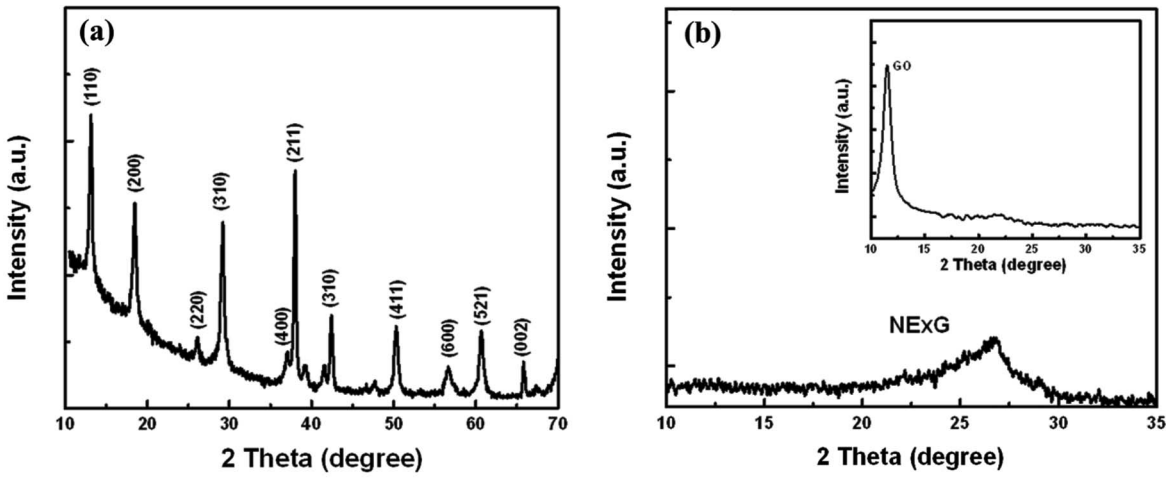

Figure 1. XRD patterns of (a) MnO_2 NT, and (b) NExG sheets (inset: graphite oxide (GO)).

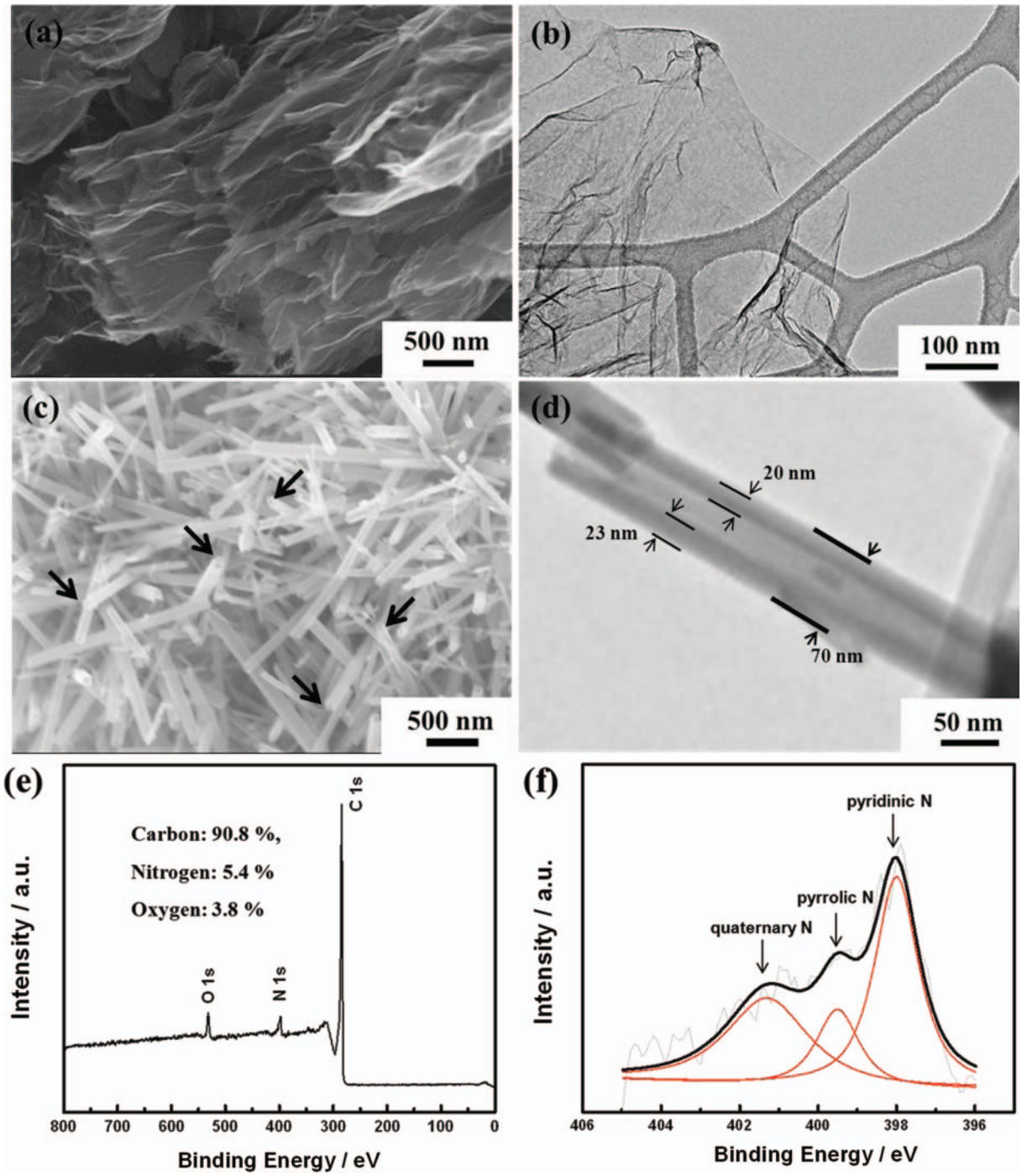

Figure 2. (a,b) SEM and TEM images of NExG sheets, (c, d) SEM and TEM images of MnO_2 NT, (e) full XPS spectrum of NExG sheets, and (f) de-convoluted high resolution N 1s XPS spectrum of NExG sheets.

percentages of the carbon, nitrogen and oxygen to be 90.8, 5.4, and 3.8%, respectively. It is assumed that the presence of O 1s peak is likely contributed to the oxygen groups of GO due to an imperfect reduction into graphene sheets, as well as oxygen adsorbed onto carbon atoms around the doped nitrogen species in graphene because nitrogen doping can generate structural defects highly active to oxygen, which is related to ORR catalysis.[14,32] The high-resolution N 1s spectrum of NExG in Figure 2f suggests the nitrogen has three different configurations, which are pyridinic N, pyrrolic N, and quaternary N with 2.5, 0.9 and 2.0% of atomic percentages, respectively, after the de-convolution of the spectrum. Quaternary nitrogen species in graphene have been reported to have influence on the ORR activity, which suggests that NExG itself also has capabilities to catalyze ORR as it is verified to contain a significant amount of 2.0% in atomic percentages of quaternary N.[29]

Electrochemical catalytic activity for ORR of the electrocatalyst has been evaluated with rotating disk electrode (RDE) system. As an aprotic non-aqueous electrolyte for Li-O_2 cell, 1 M $LiPF_6$ in TEGDME is employed as it is more widely used in recent studies due to its reasonable stability in the voltage range of interest compared to carbonated-based electrolyte that undergo relatively severe decomposition.[33–35] At first, cyclic voltammetry (CV) was carried out

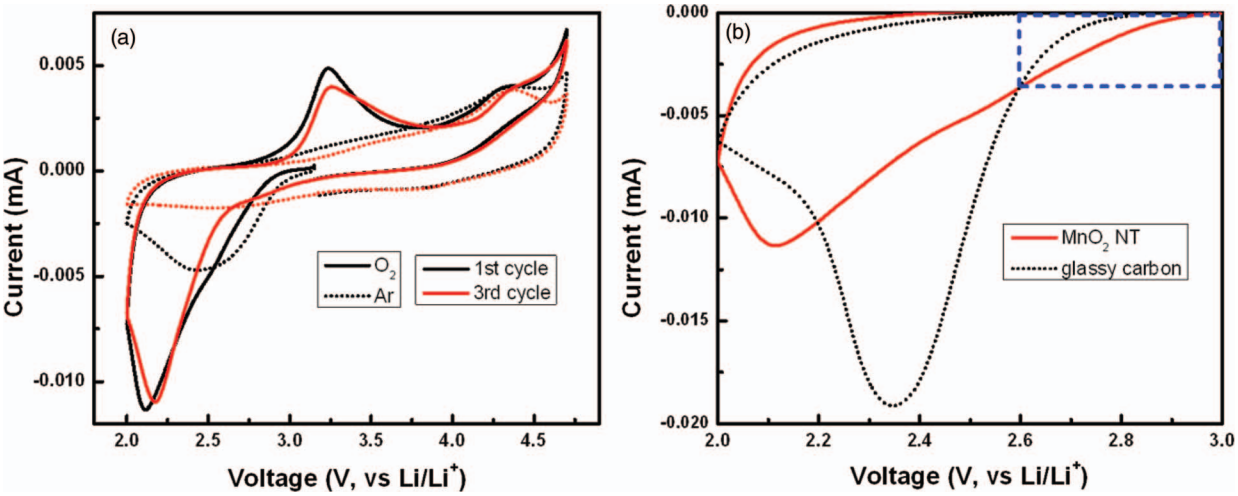

Figure 3. (a) Cyclic voltammograms of carbon-free MnO_2 NT after 1st and 3rd cycles in the potential range from 2.0 V to 4.7 V under O_2- or Ar-saturated 1M $LiPF_6$ in TEGDME and (b) ORR polarization curves of carbon-free MnO_2 NT and glassy carbon in O_2-saturated 1M $LiPF_6$ in TEGDME.

at the potential range from 2.0 V (vs. Li/Li^+) to 4.7 V starting at 3.15 V in Ar and O_2 atmosphere to investigate electrochemical behavior of a carbon-free MnO_2 NT (Figure 3a). A distinct cathodic current corresponding to ORR is observed in the first and third cycles under the O_2 atmosphere. In contrast, no significant change in the current is observed in the third cycle under the Ar atmosphere, proving that the current under the O_2 atmosphere is related to ORR. From the detailed examination of the electrochemical reaction data, the cathodic reaction is investigated using the third cycle due to the confounding effects of possible side reactions other than ORR in the first cycle. As shown in Figure 3a, the distinct cathodic current slope in the potential range of 2.6 to 3.0 V in the O_2-saturated electrolyte is observed in comparison to minimal electrochemical behavior in the Ar-saturated electrolyte, suggesting that ORR activity with MnO_2 NT is the major reaction in O_2-saturated electrolyte. There is a possible Li^+ intercalation reaction with MnO_2 in the first cycle, but this can be neglected due to the limitation of this reaction with α-MnO_2 phase according to the previously reported work.[36] Under Ar saturated electrolyte, the cathodic current observed in the first cycle might have been caused by reactions with the residual –OH functional groups which can form on α-MnO_2.[24] Further studies however are necessary in order to fully understand the exact nature of the cathodic reactions occurring during this first cycle. In addition, ORR activity of the carbon-free MnO_2 NT is compared with that of glassy carbon electrode, which was used as a substrate in the study, as shown in Figure 3b. In the potential range from 2.6 to 3.0 V, a much higher cathodic current is observed with significantly lower discharge overpotential for carbon-free MnO_2 NT compared to that of glassy carbon, which is strong evidence that the carbon-free MnO_2 NT possesses the catalytic activity for ORR. However, the limiting current of the carbon-free MnO_2 NT is lower and shifted to more negative potential compared to those of the glass carbon, presumably attributed to the low electrical conductivity of MnO_2.[22] Figure 4a presents the morphology of the MnO_2 NT/NExG composite electrode suggesting MnO_2 NT is very uniformly distributed on NExG due to its large surface area. To confirm the stability of TEGDME, cyclic voltammetry between 2.0 and 3.1 V is conducted in an Ar-saturated TEGDME. As shown in Figure 4b, no meaningful peak is observed in both the anodic and cathodic reactions associated with MnO_2 NT/NExG composite catalyst while a distinct cathodic current appears in the O_2-saturated TEGDME. Figure 5a presents ORR performances obtained by cyclic voltammetry in RDE measurements with three different carbon materials (VC, ExG and NExG) combined with MnO_2 NT including VC itself as a control material. The voltammetry sweep from 3.1 to 2.0 V in

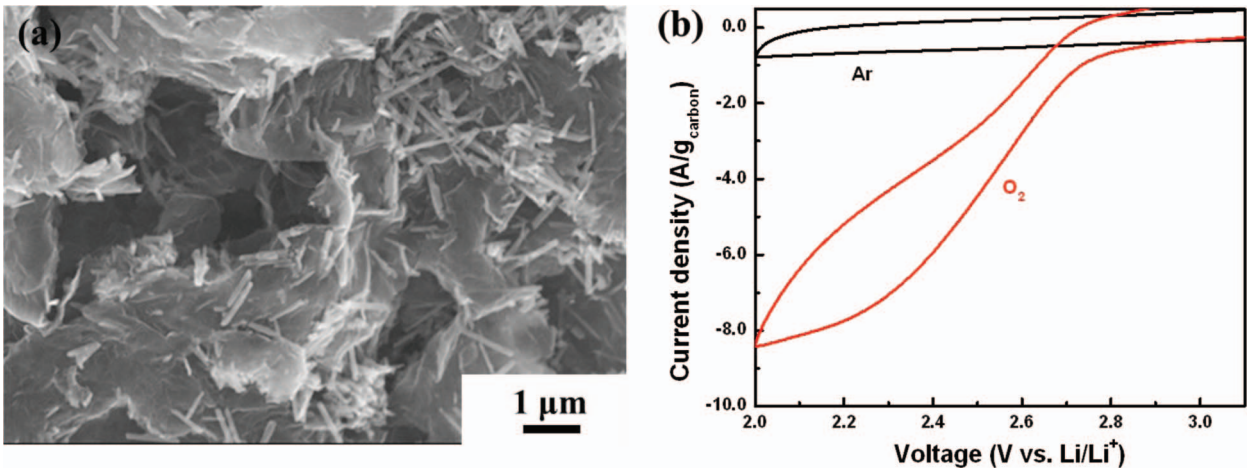

Figure 4. (a) SEM image of MnO_2 NT/NExG composite electrode, and (b) ORR polarization curve of MnO_2 NT/NExG in O_2-saturated 1 M $LiPF_6$ in TEGDME with a scan rate of 5 mV s^{-1} at a rotation rate of 900 rpm, and background scan in Ar-saturated electrolyte without any rotation.

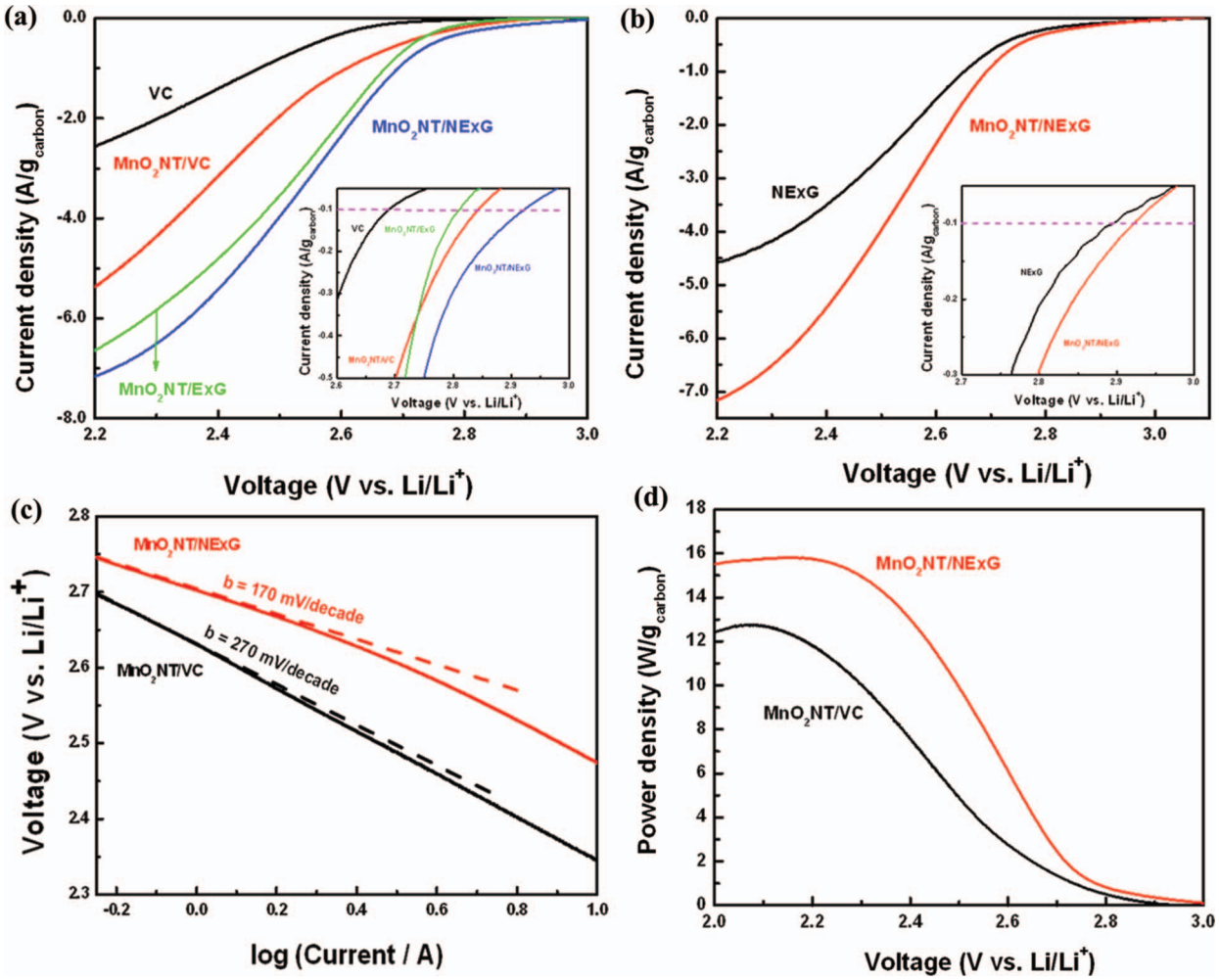

Figure 5. (a) ORR polarization curves of VC, MnO_2 NT/VC, MnO_2 NT/ExG, and MnO_2 NT/NExG in O_2-saturated 1 M $LiPF_6$ in TEGDME with a scan rate of 5 mV s^{-1} at a rotation rate of 900 rpm (inset: the current range from −0.05 to −0.5 A g^{-1}_{carbon}), (b) ORR polarization curves of NExG and MnO_2 NT/NExG with the same test conditions (inset: the current range −0.05 to −0.3 A g^{-1}_{carbon}), (c) Tafel plot and (d) power density curves of MnO_2 NT/VC and MnO_2 NT/NExG based on Figure 5a.

the negative direction is used for the examination of ORR activities at a scan rate of 5 mV s^{-1}, and a rotation rate of 900 rpm. The ORR current densities are normalized by carbon mass and background-corrected. As shown in previous reports, the cathodic currents are associated with the reduction of oxygen and combination with Li ions to form Li_2O_2 ($2Li^+ + O_2 + 2e^- \rightarrow Li_2O_2$) on the surface of carbon.[7] Vulcan carbon (VC) is first tested to investigate its catalytic activity as a starting point of the study because carbon has been widely used as a catalyst support, and the previous studies have suggested that carbon black itself could work as the ORR catalyst for Li oxygen battery.[37] The current densities in this study are normalized based on the mass of carbon supports to be consistent with other reports on Li-O_2 batteries.[7,35,38] At the current density of 100 mA g^{-1}, the potential drops to 2.69 V (Figure 5a inset), which is similar to a previously reported value.[7] The maximum current density of −2.6 A g^{-1} at 2.2 V was obtained as shown in Figure 5a. However, MnO_2 NT/VC, MnO_2 NT/ExG and MnO_2 NT/NExG composite electrodes exhibited much higher potentials at 100 mA g^{-1} which are 2.84, 2.81 and 2.92 V, respectively (Figure 5a inset). In addition, maximum current densities of the MnO_2 NT/VC, MnO_2 NT/ExG and MnO_2 NT/NExG composite electrodes increase to 5.4, 6.6 and 7.2 A g^{-1}, respectively (Figure 5a). The significantly higher onset potentials and current densities compared to those of VC verifies that MnO_2 NT combined with a carbon matrix as a composite enhances the ORR activity in an aprotic electrolyte with the higher reaction potential, and high current density for Li-O_2 battery. MnO_2 NT has previously been reported as a superior ORR catalyst in an aqueous alkaline solution compared to MnO_2 with nanorod morphology because of its larger surface area.[20] However, this is the first study to employ MnO_2 NT to investigate the ORR performance in an aprotic medium for Li-O_2 battery. Furthermore, the graphene supported MnO_2 NT electrodes show a higher electrocatalytic activity in terms of the current density in the lower potential range compared to the MnO_2 NT/VC, suggesting higher surface area and electrical conductivity contributed by the graphene sheets can enhance the rate of reaction related to O_2 mass diffusion and provide more sites for the deposition of Li_2O_2. In the higher potential range, however, the ORR potential of MnO_2 NT/ExG at 100 mA g^{-1} is observed even lower than that of MnO_2 NT/VC, which is an indication that the contribution of ExG toward ORR is insignificant. The catalytic activity of ExG is improved by doping the graphitic network with nitrogen atoms, which resulted in an increase in both the kinetics of ORR and limiting current density as shown in Figure 5a and 5b. These improvements are strong evidence at not only MnO_2 NT is catalytically active, but also NExG enhances the activity toward ORR, confirming the important of nitrogen species in the graphene sheets that enhance the catalytic capability of the metal oxide in an aprotic Li-O_2 cell. It is proposed that nitrogen doping of graphitic carbon materials shows dramatic enhancements in catalytic for ORR as demonstrated

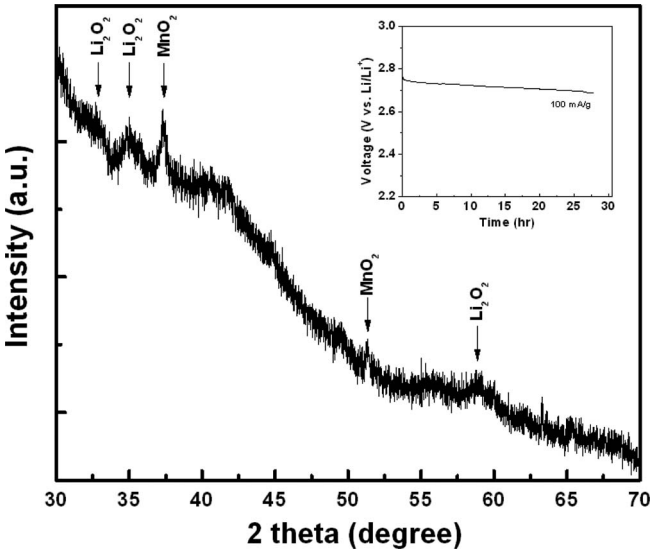

Figure 6. XRD pattern of the MnO_2 NT/NExG electrode after ORR studies. (inset: voltage vs. time profile obtained by galvanostatic test at the current density of 100 mA g^{-1}_{carbon})

previously for carbon nanotubes[39,40] and graphene materials.[14,32,41] This is attributed to the variations in electronic properties, oxygen binding energies and surface adsorption properties. To confirm this hybrid effect of MnO_2 NT/NExG composite, the performance of NExG itself was compared as shown in Figure 5b. It exhibits 2.89 V at 100 mA g^{-1} and 4.6 A g^{-1} at 2.2 V, which are evidence of increased catalytic activity compared those of VC. This is consistent with results from previous reports;[14] however, the performance of NExG itself are observed to be less than that of MnO_2 NT composited with NExG. It verifies that NExG combined with MnO_2 NT results in the highest hybrid effect for ORR in an aprotic electrolyte for Li-O_2 battery. Furthermore, the Tafel plot in Figure 5c confirms a superior ORR kinetics of MnO_2 NT/NExG by demonstrating a smaller Tafel slope of 170 mV/decade than that of MnO_2 NT/VC (270 mV/decade).[42] To further demonstrate excellent activity of MnO_2 NT/NExG, the power density of MnO_2 NT/NExG is calculated and compared with MnO_2 NT/VC as shown in Figure 5d. The power density of MnO_2 NT/NExG demonstrates a maximum of 15.8 W g−1 at 2.19 V which is 32% higher than that of MnO_2/VC (12.0 W g^{-1}) at the same voltage, supporting the faster kinetics of ORR in the Li-O_2 cell. The X-ray diffraction (XRD) pattern of the electrode after the discharge exhibits the patterns of the discharge product Li_2O_2 with the detection of MnO_2 NT as shown in Figure 6, which is consistent with the previously reported work.[43] It should be note that before conducting XRD, a galvanostatic test for discharge with 100 mA g^{-1} of current density was carried out to accumulate Li_2O_2 (Figure 6 inset).

Conclusions

In this study, we introduced α-MnO_2 NT incorporated NExG composite material as the air cathode for Li-O_2 battery applications. While MnO_2 NT/VC demonstrates a remarkable electrochemical performance with 2.84 V at the current density of 100 mA g^{-1}, NExG prepared by the simple one step method shows a superior hybrid ORR activities when combined with MnO_2 NT, shifting the voltage at 100 mA g^{-1} of the current density to a more positive value of 2.92 V. In addition, the current density obtained in the RDE studies is twice higher than that of MnO_2 NT/VC with 32% higher maximum power density. The increased ORR activity is most likely due to the defect sites generated by nitrogen doping resulting in a highly voile-like 2-D morphology with superior electronic property of the graphene sheets. The results from this study is a demonstration of a rational way to improve the ORR performance by employing NExG in combination with metal oxide such as MnO_2 NT to create an efficient composite electrocatalyst for highly promising Li-O_2 batteries.

Acknowledgments

This research was supported by the Natural Sciences and Engineering Research Council of Canada (NSERC) through grants to Dr. Zhongwei Chen and Dr. Linda F. Nazar, the Waterloo Institute for Nanotechnology and the University of Waterloo.

References

1. K. M. Abraham and Z. Jiang, *Journal of the Electrochemical Society*, **143**, 1 (1996).
2. T. Ogasawara, A. Debart, M. Holzapfel, P. Novak, and P. G. Bruce, *Journal of the American Chemical Society*, **128**, 1390 (2006).
3. G. Girishkumar, B. McCloskey, A. C. Luntz, S. Swanson, and W. Wilcke, *Journal of Physical Chemistry Letters*, **1**, 2193 (2010).
4. P. G. Bruce, S. A. Freunberger, L. J. Hardwick, and J. M. Tarascon, *Nature Materials*, **11**, 19 (2012).
5. J. Christensen, P. Albertus, R. S. Sanchez-Carrera, T. Lohmann, B. Kozinsky, R. Liedtke, J. Ahmed, and A. Kojic, *Journal of the Electrochemical Society*, **159**, R1 (2012).
6. J. S. Lee, S. T. Kim, R. Cao, N. S. Choi, M. Liu, K. T. Lee, and J. Cho, *Advanced Energy Materials*, **1**, 34 (2011).
7. Y. C. Lu, H. A. Gasteiger, and Y. Shao-Horn, *Journal of the American Chemical Society*, **133**, 19048 (2011).
8. J. Wu, H. W. Park, A. P. Yu, D. Higgins, and Z. W. Chen, *Journal of Physical Chemistry C*, **116**, 9427 (2012).
9. Y. W. Zhu, M. D. Stoller, W. W. Cai, A. Velamakanni, R. D. Piner, D. Chen, and R. S. Ruoff, *Acs Nano*, **4**, 1227 (2010).
10. A. P. Yu, H. W. Park, A. Davies, D. C. Higgins, Z. W. Chen, and X. C. Xiao, *Journal of Physical Chemistry Letters*, **2**, 1855 (2011).
11. G. H. Yu, L. B. Hu, N. A. Liu, H. L. Wang, M. Vosgueritchian, Y. Yang, Y. Cui, and Z. A. Bao, *Nano Letters*, **11**, 4438 (2011).
12. E. Yoo and H. S. Zhou, *Acs Nano*, **5**, 3020 (2011).
13. Y. L. Li, J. J. Wang, X. F. Li, D. S. Geng, R. Y. Li, and X. L. Sun, *Chemical Communications*, **47**, 9438 (2011).
14. Y. L. Li, J. J. Wang, X. F. Li, D. S. Geng, M. N. Banis, R. Y. Li, and X. L. Sun, *Electrochemistry Communications*, **18**, 12 (2012).
15. Z. H. Sheng, H. L. Gao, W. J. Bao, F. B. Wang, and X. H. Xia, *Journal of Materials Chemistry*, **22**, 390 (2012).
16. H. B. Wang, T. Maiyalagan, and X. Wang, *Acs Catalysis*, **2**, 781 (2012).
17. Z. Yang, Z. Yao, G. F. Li, G. Y. Fang, H. G. Nie, Z. Liu, X. M. Zhou, X. Chen, and S. M. Huang, *Acs Nano*, **6**, 205 (2012).
18. L. Wang, X. Zhao, Y. H. Lu, M. W. Xu, D. W. Zhang, R. S. Ruoff, K. J. Stevenson, and J. B. Goodenough, *Journal of the Electrochemical Society*, **158**, A1379 (2011).
19. H. L. Wang, Y. Yang, Y. Y. Liang, G. Y. Zheng, Y. G. Li, Y. Cui, and H. J. Dai, *Energy & Environmental Science*, **5**, 7931 (2012).
20. W. Xiao, D. L. Wang, and X. W. Lou, *Journal of Physical Chemistry C*, **114**, 1694 (2010).
21. G. Q. Zhang, J. P. Zheng, R. Liang, C. Zhang, B. Wang, M. Au, M. Hendrickson, and E. J. Plichta, *Journal of the Electrochemical Society*, **158**, A822 (2011).
22. F. Y. Cheng and J. Chen, *Chemical Society Reviews*, **41**, 2172 (2012).
23. H. Cheng and K. Scott, *Journal of Power Sources*, **195**, 1370 (2010).
24. F. Y. Cheng, Y. Su, J. Liang, Z. L. Tao, and J. Chen, *Chemistry of Materials*, **22**, 898 (2010).
25. Z. Chen, A. P. Yu, R. Ahmed, H. J. Wang, H. Li, and Z. W. Chen, *Electrochimica Acta*, **69**, 295 (2012).
26. A. Abouimrane, O. C. Compton, K. Amine, and S. T. Nguyen, *Journal of Physical Chemistry C*, **114**, 12800 (2010).
27. D. S. Geng, S. L. Yang, Y. Zhang, J. L. Yang, J. Liu, R. Y. Li, T. K. Sham, X. L. Sun, S. Y. Ye, and S. Knights, *Applied Surface Science*, **257**, 9193 (2011).
28. H. L. Guo, X. F. Wang, Q. Y. Qian, F. B. Wang, and X. H. Xia, *Acs Nano*, **3**, 2653 (2009).
29. D. S. Geng, Y. Chen, Y. G. Chen, Y. L. Li, R. Y. Li, X. L. Sun, S. Y. Ye, and S. Knights, *Energy & Environmental Science*, **4**, 760 (2011).
30. M. J. McAllister, J. L. Li, D. H. Adamson, H. C. Schniepp, A. A. Abdala, J. Liu, M. Herrera-Alonso, D. L. Milius, R. Car, R. K. Prud'homme, and I. A. Aksay, *Chemistry of Materials*, **19**, 4396 (2007).
31. D. C. Wei, Y. Q. Liu, Y. Wang, H. L. Zhang, L. P. Huang, and G. Yu, *Nano Letters*, **9**, 1752 (2009).
32. L. T. Qu, Y. Liu, J. B. Baek, and L. M. Dai, *Acs Nano*, **4**, 1321 (2010).
33. C. O. Laoire, S. Mukerjee, E. J. Plichta, M. A. Hendrickson, and K. M. Abraham, *Journal of the Electrochemical Society*, **158**, A302 (2011).
34. H.-G. Jung, J. Hassoun, J.-B. Park, Y.-K. Sun, and B. Scrosati, *Nature Chemistry*, **4**, 579 (2012).
35. J.-H. Lee, R. Black, G. Popov, E. Pomerantseva, F. Nan, G. A. Botton, and L. F. Nazar, *Energy & Environmental Science*, **5**, 9558 (2012).
36. M. M. Thackeray, *Progress in Solid State Chemistry*, **25**, 1 (1997).
37. B. D. McCloskey, R. Scheffler, A. Speidel, D. S. Bethune, R. M. Shelby, and A. C. Luntz, *Journal of the American Chemical Society*, **133**, 18038 (2011).

38. S. R. Lee, H. M. Kim, K. Char, J. H. Jang, M. Kim, M. R. Cho, Y. D. Park, R. Jung, D. C. Kim, and S. Seo, *Current Applied Physics*, **12**, 369 (2012).
39. Z. Chen, D. Higgins, H. S. Tao, R. S. Hsu, and Z. W. Chen, *Journal of Physical Chemistry C*, **113**, 21008 (2009).
40. S. M. Zhu, Z. Chen, B. Li, D. Higgins, H. J. Wang, H. Li, and Z. W. Chen, *Electrochimica Acta*, **56**, 5080 (2011).
41. Y. Wang, Y. Y. Shao, D. W. Matson, J. H. Li, and Y. H. Lin, *Acs Nano*, **4**, 1790 (2010).
42. Y. C. Lu, H. A. Gasteiger, and Y. Shao-Horn, *Electrochemical and Solid State Letters*, **14**, A70 (2011).
43. R. Black, S. H. Oh, J. H. Lee, T. Yim, B. Adams, and L. F. Nazar, *Journal of the American Chemical Society*, **134**, 2902 (2012).